International Journal of Recent Engineering Science (IJRES)
ISSN: 2349 – 7157 / doi: 10.1445/23497157/IJRES-V7I2P104

Volume 7 Issue 2, 17-21, Mar-Apr 2020

Improve Multidimensional 5G OFDM Based MIMO Sushisen Algorithms Merge Multi-Cell Transmission

P. Senthil[1], Stanly[2], M.Suganya[3], S.S.Inakshi[4]
[1]*Associate Professor, Department of Computer Science, Kurinji College of Arts and Science, Tiruchirappalli, Tamilnadu*
[2]*Principal & Secretary, S.B.T College of Special Education, Madurai, Tamilnadu*
[3]*Department of English, Cresent School, Tiruchirappalli, Tamilnadu*
[4]*Department of Science, YMCA School, Tiruchirappalli, Tamilnadu*

Abstract

Wireless communication industry in the last decade, there is a need for techniques to reliably communicate at higher data rates and efficiently use the available bandwidth. One such technology is the use of multiple antennas at both transmitter and receiver sites of wireless communication systems known as multiple-input – multiple-output (MIMO) communication system. In MIMO systems, the information signal at both sides of the communication link is combined so that the quality (bit-error-rate) or data rates (bit-per-sec) is improved. The paper provides a study for different diversity gain coding schemes and spatial multiplexing coding for MIMO systems. A comparison of various channel estimation and equalization techniques are given. The simulation is implemented using MATLAB, and the results had shown the performance of transmission models under different channel environments.

Keywords: *MATLAB MIMO, Cell Phone Network*

I. INTRODUCTION

This paper evaluates the bit error rate (BER) performance of the MIMO-OFDM communication system. MIMO system uses multiple transmitting and receiving antennas with different coding techniques to enhance the transmission diversity or spatial multiplexing gain. Utilizing the alamouti algorithm was the same information is transmitted over multiple antennas in different time intervals and then collected again at the receivers to minimize the probability of error, combat fading, and thus improve the received signal to noise ratio. While utilizing the V-BLAST algorithm, the transmitted signals are divided into different transmitting channels and transferred over the channel to be received by different receiving antennas to increase the transmitted data rate and achieve higher throughput.

The paper starts in section 2 to introduce a model for the MIMO system; section 3 provide different coding methods: Space-time block codes and spatial multiplexing codes, section 4 provide methods for evaluating the diversity and MIMO performance, section 5 simulation results are provided to measure the system performance, and finally in section 6 a conclusion is being provided.

II. REVIEW OF WORKS

The input binary data are first modulated by generating complex symbols taking values in a finite alphabet corresponding to a digital modulation type (BPSK, QPSK, QAM), then demultiplexed into N.T. parallel symbol stream (Foschini, 1996).VBLAST transmission the binary data stream are demultiplexed into N.T. parallel sub-streams (layers), each is modulated (BPSK, QPSK, M-QAM) and transmitted over the N.T. antenna (Rao, 2015).

The multiple-receive antenna array, also called the adaptive antenna array (A.A.A.), can be used in OFDM for interference suppression. A.A.A. techniques have first been proposed for narrow-band TDMA in [41] to suppress cochannel interference. A comprehensive introduction of A.A.A. techniques and beamforming can be found in [42].

III. PROBLEM AND RESEARCH WORKS

In the orthogonal frequency division multiplexing (OFDM), the peak power might be much larger than the average power due to adding up subcarriers coherently, resulting in a large peak-to-average power ratio (PAPR). PAPR is a very important communication system because it has big effects on the transmitted signal. Low PAPR makes the transmit power amplifier works efficiently; on the other hand, the high PAPR makes the signal peaks move into the non-linear region of the R.F. power amplifier, which reduces the efficiency of the R.F. power amplifier. Besides, high PAPR requires a high-resolution digital- to- analog converter (D.A.C.) at the transmitter, high-resolution analog -to -digital converter (A.D.C.) at the receiver. Any non-linearity in the signal will cause distortion, such as inter-carrier interference (I.C.I.) and inter-symbol interference (I.S.I.). Thus, OFDM signals have a very large peak to average power ratio. In the transmitter, the maximum output power of the amplifier limits the peak amplitude of the signal. This effect produces interference both within the OFDM band and in adjacent frequency bands. A high peak-to-average-power ratio (PAPR) has been cited as one of the drawbacks of the OFDM modulation format. In the R.F. systems, the major problem resides in the transmitter end's power amplifiers, where the amplifier gain will saturate at high input power [17]. One way to avoid the relatively

"peaky" OFDM signal is to operate the power amplifier at the so-called heavy "back-off" mode, where the signal power is much lower than the amplifier saturation power. Unfortunately, this requires an excess large saturation power for the power amplifier, leading to low power efficiency [40]. The amplitude threshold is shown in Fig. 4.1, in which, few peaks of OFDM signal cross that threshold limit. It is due to the non-linear behavior of the amplifier at the transmitter end.

IV. IMPLEMENTATION AND CLASSIFICATION

The peak to average power ratio of the OFDM signal is defined as the ratio of the maximum peak power divided by the average power of the OFDM signal [11]. It is critical in OFDM. Consider a non OFDM system or single carrier system with QPSK modulated symbols x(0), x(1), x(2)...and so on & power in each symbol is equal to a2 (i.e., the peak power). Now the average power is given as-

- PAPR & P.A.R.: Peak-To-Average Power Ratio
- PMEPR: Peak-To-Mean Envelope Power Ratio
- Crest factor of x(t): square root of PAR
- Definition: PAR = (||x||∞)2 / E[(||x||2) 2]
- average power = E {|x (k)|2}=a2 [k = 0,1,2….] 4.1

Hence, in a single carrier system both, the peak power and the average power are equals and given by a2. Now from the definition of PAPR "Ratio of peak power to average power" and given by the expression:

PAPR= Peak power/Average Power 4.2

PAPR= a2/ a2 4.3

PAPR= 1 4.4

From the above equation, it is clear that for a single carrier system, the PAPR is equal to 1 or 0 dB. Nevertheless, practically, it is closed to unity. It is also clear that there is no significant deviation from the mean power level.

For OFDM system or in multicarrier modulation scheme consider that the transsmitted samples are x(0), x(1), x(2)…… x(N-1) which are the IFFT samples of information symbols X(0), X(1), X(2)…… ……X(N-1) [17] and [39]. Now from the expression of kth IFFT sample givenas Now the average power is:

Average power = E {|x (k) |2}
={|x(i)|E{|x(i)|square}×E{|eN +square}

Where {|ej2π(ki/N)|square} is the phase factor and its value is unity or 1.

Or E {|x (k)|2} = a2/N 4.9

Since the peak power in the multicarrier modulation scheme is also a2. Hence, from the definition of PAPR,i.e.-

PAPR = Peak power/Average Power
Or PAPR = a2/(a2/N)
Or PAPR = N 4.10

It is clear from equation 3.10 that, for a multicarrier system, the PAPR is equal to the N. It means in a multicarrier environment, PAPR is equaled to the number of subcarriers and can be significantly high. The high PAPR in an OFDM system is essential arises because of the IFFT operation at the transmitter. Data symbols across subcarrier can add up to produce a high peak value signal [40] and [49].

Superimposing the continuous-time baseband OFDM signal with the radio frequency signal (also called carrier signal) introduces a continuous-time pass band OFDM signal. It does not change the peak power, but the average power of the passband OFDM signal is half the average power of the continuous-time baseband OFDM signal [39]. Thus, the PAPR of the continuous-time passband signal is generally larger than that of the continuous-time baseband OFDM signal by three dB [17]. The relationship between PAPR of discrete-time baseband OFDM signal [PAPR(an)], PAPR of continuous-time baseband OFDM signal [PAPR(an)] and PAPR of continuous-time pass band OFDM signal [PAPR (gt)] are given as [11] and [39]:

PAPR(an) ≤ PAPR(an) < PAPR (gt)

So, as per the introduction of PAPR, it is concluded that the reduction of PAPR is the most important point for the OFDM system.

V. EXECUTION AND RESULTS

The mechanism of electromagnetic wave propagation reveals that, in free space, the strength of a transmitted signal decays with a rate that is inversely proportional to the travel distance's square. The simplest explanation is to consider an Omni-directional antenna. The emitted power transmits in all directions. The perceived power density in a unit area is then inversely proportional to the travel distance's square. In a realistic environment, the transmitted signal encounters obstructions so that it is not attenuated in the same way as in free space. However, the fundamental physical rules teach us that the signal strength is still decaying with increasing travel distance in a certain manner.

$$x_k = \sum_{n=0}^{L} h_n u_{k-n}$$

$$u(t) = \mathrm{Re}\left[e^{-j2\pi f_0 t} \sum_{k=1}^{N-1} e^{-j2\pi k f_0 t + \delta_k} \right]$$

$$u(t) = \mathrm{Re}\left[e^{-j2\pi t/T} \sum_{k=1}^{N-1} s_k e^{-j2\pi k t/T} \right] = \mathrm{Re}\left[e^{-j2\pi t/T} S(t) \right]$$

$$S(t)=\sum_{k=0}^{N-1} s_k e^{-j2\pi kt/T} \xleftrightarrow{\text{Fourier Transform}} \{S_k\}$$

$$\overline{X}=H\overline{U},\quad H=\begin{pmatrix} h_L & h_{L-1} & \cdots & h_0 & 0 & \cdots & 0 & 0 \\ 0 & h_L & h_{L-1} & \cdots & h_0 & 0 & \cdots & 0 \\ \vdots & \ddots & \ddots & \ddots & \ddots & \ddots & \ddots & 0 \\ \vdots & \ddots & \ddots & \ddots & \ddots & \ddots & \ddots & 0 \\ 0 & \cdots & 0 & 0 & h_L & h_{L-1} & \cdots & h_0 \end{pmatrix}$$

$$H_o=\begin{pmatrix} h_o & O & O & \cdots & O \\ \vdots & h_o & O & \cdots & O \\ h_L & \cdots & \ddots & \cdots & \vdots \\ \vdots & \ddots & \cdots & \ddots & O \\ O & \cdots & h_L & \cdots & h_o \end{pmatrix}$$

$$H_1=\begin{pmatrix} O & \cdots & h_L & \cdots & h_1 \\ \vdots & \ddots & O & \ddots & \vdots \\ O & \cdots & \ddots & \cdots & h_L \\ \vdots & \ddots & \cdots & \ddots & O \\ O & \cdots & O & \cdots & O \end{pmatrix}$$

$$X(i)=H_o U(i)+H_1 U(i-1)+\eta(i)$$

$U(i)$: ith transm itted block
$U(i-1)$: (i -1)th trans mitted block
$X(i)$: ith received block
$\eta(i)$: noise vector

(It is the equation used transmission data block analysis)

4.5.1 Shadow Fading

The fading shadow term considers the environmental clusters where the transmitter and the receiver reside, respectively. The shadowing term simulates various effects introduced due to the obstructions encountered in the radio propagation, such as reflection, diffraction. Inherently, shadow fading is a random loss around the average loss specified by the distance-dependent loss. Measurements have shown that a log-normal distribution describes the effect of shadow fading well. Thus, the path loss can be expressed by

$$P_e=\left(G_c \cdot SNR\right)^{-G_d}$$

G_c --- Coding gain

G_d -Diversity gain

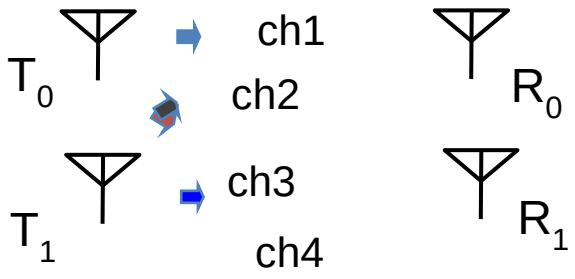

Fig 1: sender to receiver processing LTE-A

fig 1 At the receiver, multiple antennas receive signals from each(T0, T1) antenna. The baseband representation of a received signal vector for (R0, R1) band can be expressed P.L.

T0 = Simplest implementation is orthogonal space time block codes , and Alamouti codes
(T1).R1 = Transmitter sends
R2 = multiple signals

Sushisen Algorithms

1. GenDecTree(pattern S, features F)
2. If stopping_condition(S,F) = actual then
3. leaf = createNode()
4. leaf.label= Classify(S)
5. return leaf
6. root = createNode()
7. root.test_condition = findBestSplit(S,F)
8. V = v a possible outcome of root.test_condition
9. for every price vϵV:
10. Sv: = root.test_condition(s) = v and s ϵ S;
11. toddler = GenDecTree(Sv ,F) ;
12. upload infant as a descent of root and label the edge (root□baby) as v
13. return root
14. feature dr = transceive(toes, d2s)
15. Initialization
16. continual hrx htx; dr=complicated(zeros(nspf,1)); ns=zero;
17. if isempty(hrx), hrx = ...; htx = ...;
18. give up
19. if ~toes
20. Transmit one body
21. step(htx,d2s);
22. receive one frame the usage of polling
23. at the same time as (ns == 0), [dr,ns] = step(hrx); end
24. Termination
25. else, release(hrx); launch(htx); cease

Table 1: Parameters of the AWGN II B3 Path Loss Model

BS height	6 m
MS height	1.5 m
Distance d ,m-	5 m < d < 100 m
LOS path loss	A = 13.9 B = 64.4 C = 20
NLOS path loss	A = 37.8 B = 36.5 C = 23
L.O.S. shadow fading std.,dB-	3 dB
NLOS shadow fading std.,dB-	4 dB

Where T is the path loss exponent indicating the rate at which the path loss increases with distance, is a zero-mean Gaussian distributed random variable (in dB) with standard deviation, and(∑) is the loss measured from a reference distance(#).

Multipath Fading

Multipath fading is used to describe the rapid fluctuations of the received signal strength over a short movement. This is induced by the fact that the received signal is the sum of interfering signals arriving at different times. The difference in the interfering signals' arrival time is because they arrive at the receiver via different transmission paths. In systems with a carrier frequency in the order of Giga Hz, a movement of the receiver in the order of one meter is more than enough to bring the channel from a constructive interference to a destructive interference situation.

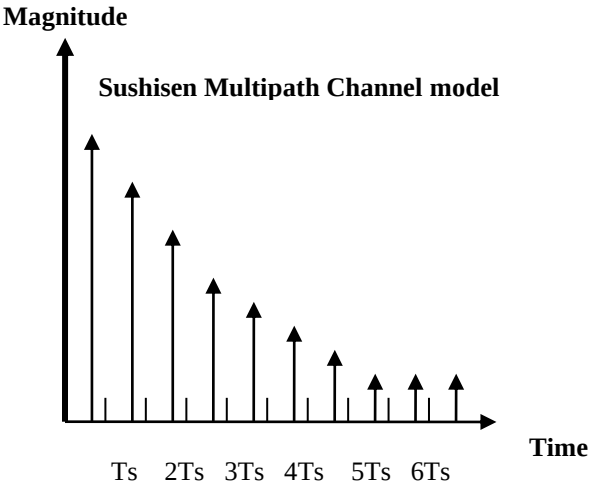

Fig 2: Sushisen Multipath channel model

In the high SNR regions, fig 4.4, there is a more substantial effect of increasing diversity on the performance. A good agreement between the analytical and simulation results in the multipath Rayleigh fading channel validates.

Table 2:Overall analysis MIMO OFDM

Eb/No (db)	BER in AWGN	BER in Rayleigh	BER in Rician
-3	0.1584	0.2107	0.150
0	0.07865	0.1464	0.06
5	0.005954	0.06414	0.005
8	0.0001909	0.03536	0.0008
9	0.00003363	0.02901	0.00004
10	--	0.02323	--

$$s_{CAZAC}(km+l) = \exp\left(i2\pi \frac{mc(s)\alpha(l)k^2 + \beta(l)k + \gamma(l)}{sm}\right) \text{..... ..(1)}$$

$\forall l \in Z_m$ and $\forall k \in Z_{sm}$,

where

$c(s) = \begin{cases} 1/2 & \text{if } \bmod(s,2) = 0 \\ 0 & \text{otherwise} \end{cases}$,

$\alpha(l) \in Z_s^*, \forall l \in Z_m$, is any function with $\gcd(\alpha(l), s) = 1$,

$\beta(l) \in Z_{sm}, \forall l \in Z_m$, is any function such that $\bmod(\beta(l), m)$ is a permutation of Z_m,

$\gamma(l), \forall l \in Z_m$, is any rational number.

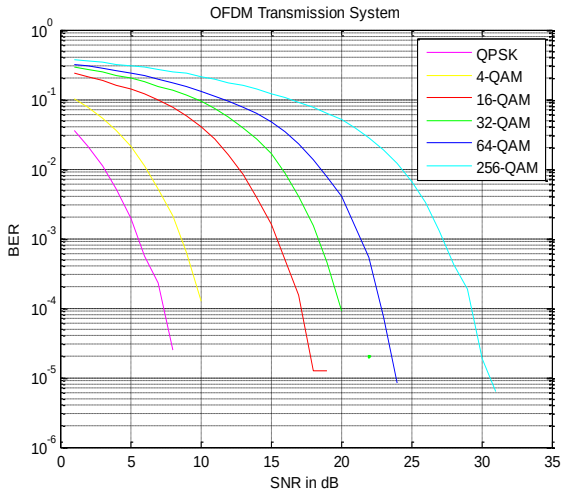

Fig 3: Result Sushisen Multipath channel

VI. CONCLUSION

From the above simulation results, it is proved that the proposed MIMO algorithm has improved the performance by the correction of fractional value in the system. Though Turbo codes give better results than convolution codes, the results can still further be improved employing power optimization. The transmit power can be optimized in order to avoid the power allocation to the frequency nulls. The capacity of an OFDM mobile radio link can be significantly increased using adaptive transmission techniques. For SISO systems, adaptive modulation can be utilized to adapt the transmission scheme to the radio channel as well as possible. In the case of systems with multiple antennas, in addition to the modulation scheme also the MIMO scheme can be adapted to the radio channel. The main drawback of adaptive modulation is that it requires sushisen algorithm synchronization between transmitter and receiver concerning the modulation scheme. Low PAPR results for the proposed type of preambles have been obtained for various decimation factors 1,2,3,4 (corresponding to 1, 2, 3, and 4 repetitions of P.N. sequences) and FFT size = 2K, 4K, and 6K. These confirm that the desirable properties of the proposed preambles can be maintained independently of the choice of preamble structures.

ACKNOWLEDGEMENTS

This paper is made possible varagupady or varagupadi in Perambalur TamilNadu through the help and support from everyone, including My friend M.suganya and Daughter S.S.Inakshi, and in essence, all sentient beings. I sincerely thank my parents, family, and

friends who provide advice and financial support. The product of this paper would not be possible without all of them.

REFERENCES

[1] Marzetta TL Noncooperative cellular wireless with unlimited numbers of base station antennas, IEEE Trans Wirel Commun. 9(11) (2010) 3590–3600.

[2] Rusek F, Larsson EG, Marzetta TL., Scaling up MIMO: opportunities and challenges with very large arrays, IEEE Signal Process Mag. 30(1) (2013) 40–60.

[3] Larsson EG, Edfors O, Tufvesson F.,Massive MIMO for next-generation wireless systems, IEEE Commun Mag. 52(2) (2014) 186–195.

[4] Lu L, Li GY, Swindlehurst AL., An overview of massive MIMO: benefits and challenges, IEEE J Sel Topics Signal Process 8(5) (2014) 742–758.

[5] Marzetta TL., Massive MIMO: an introduction. Bell Labs Tech J 20 (2015) 11–22.

[6] Senthil, P., Enhanced of Image Mining Techniques the Classification Brain Tumor Accuracy (ENCEPHALON), International Journal of Computer Science and Mobile Computation. 5(5) (2016) 110-115.

[7] Senthil, P., Medicine Neural Networks Control Mind of Memory in Image Processing (Men-Net-Mind), International Journal of Modern Computer Science (IJMCS) .4(2) (2016) 150-156.

[8] Senthil, P., Discovery of Image Mining used Brain Tumor using Improve Accuracy and Time (ANGIOGRAPHY), International Journal of Modern Computer Science and Applications (IJMCSA).4(3) (2016) 28-33.

[9] Senthil, P., Image Mining Using Attribute Supported Brain Tumor Synthesis by DWT (M.R.I. Relevance), International Journal of Modern Computer Science and Applications (IJMCSA). 5(3) (2016) 85-90.

[10] Senthil, P., Brain Tumors Frequency Image Mining Used Detection Time Technique in Medical Images, International Journal of Modern Electronics and Communication Engineering (IJMECE).4(3) (2016) 39-45.

[11] Senthil, P., Image Mining Using Lipomatous Ependymoma on Weighted Image Find Brain Tumor (Allin One), International Journal of Modern Computer Science (IJMCS).4(6) (2016) 12-18.

[12] Senthil, P., Image Mining Automata Based Seeded Tumor C-Taxonomy Algorithm for Segmentation of Brain Tumors on M.R. Images (BITA), Asian Journal of Computer Science and Technology. 5(1) 2016 1.

[13] Senthil, P., An Improved Gradient Boosted Algorithms Based Solutions Predictive Model (Trade), Asian Journal of Managerial Science. 5(1) (2016) 30-40.

[14] Senthil, P., Image Mining Brain Tumor Detection using Tad Plane Volume Rendering from M.R.I. (IBITA), Journal of Computer - JoC, Available Online at: www. journal. Computer. 1(1) (2016) 1-13.

[15] Senthil, P., ENHANCED BIG DATA CLASSIFICATION SUSHISEN ALGORITHMS TECHNIQUES IN HADOOP CLUSTER (META), Journal of Computer - JoC, Available Online at: www. journal. Computer. 1(1) (2016) 14-20.

[16] Senthil, P., IMAGE MINING USED SEGMENTATION TECHNIQUE MRI SCAN BRAIN TUMOR IMAGES ANALYSIS (IMUSA), Journal of Computer - JoC, Available Online at: www. journal. Computer.1(1).

[17] Senthil, P., IMAGE MINING CLASSIFICATION MRI SCAN USED BRAIN TUMOR ANALYSIS (IMICLA), Journal of Computer – JoC.1(1) (2016) 21-35.

[18] Senthil, P., IMAGE MINING EFFECT USING GAUSSIAN SMOOTH IN BRAIN TUMOR INCREASING THE SEGMENTING ACCURACY (I- MENINGIOMA), Journal of Computer – JoC. 1(2) (2016) 63-73.

[19] Senthil, P., Image Mining Base Level Set Segmentation Stages To Provide An Accurate Brain Tumor Detection, International Journal of Engineering Science and Computing. 6(7) (2016) 8295-8299.

[20] Senthil, P., Image Mining Brain Tumor Detection using Tad Plane Volume Rendering from M.R.I. (IBITA), Journal of computer science.1(1) (2016) 1-13.

[21] Senthil, P., Image Mining Brain Tumor Detection using Tad Plane Volume Rendering from M.R.I. (IBITA), journal of computer Science.1(1) (2016) 1-13.

[22] Senthil, P.,Image Mining in Fuzzy Model Approaches Based Random walker algorithm Brain Tumor Analysis (Meningioma Analysis), International Journal of Computer Science & Engineering Technology (IJCSET).7(7) (2016) 303 – 315.

[23] Senthil, P., IMAGE MINING USING DISEASE ACCURACY ANALYSIS (Muda), International Research Journal of Engineering and Technology (IRJET). 3(6) (2016) 309-318.

[24] Senthil, P., EXPOSURE WITH CREDENTIALS OF BRAIN TUMOR USING IMAGE MINING MICCAI PERFORMANCE (MELANOMA), International Journal of Current Research. 8(8) (2016) 36002-36006.

[25] Senthil, P., Image Mining in Tumor Detection in Brain using Sushisen in Arima Model Indian Journal Of Natural Sciences. 3(7) (2016) 11480-11496.

[26] Senthil, P., Image Mining Segmentation Adaboost Glioma Prevents Progression to High-Grade Glioma Accuracy(Image), International Journal of Engineering Studies and Technical Approach (IJESTA).2(9) (2016) 1-10.

[27] Senthil, P., Templaste and Inasu algorithms using Medical images Analysis,International Journal of Engineering Studies, and Technical Approach (IJESTA).2(10) (2016).

[28] Senthil, P., Image Mining In ranking Approach under Interval-Valued Hesitant Fuzzy Set Gr Selection, International Journal of Scientific Research in Computer Science, Engineering and Information Technology.1(2) (2016) 105-114.

[29] Senthil, P., Cancer Detection Cancer and Classification Radiotherapy Treatment, International Journal of Engineering Studies and Technical Approach (IJESTA). 2(12) (2017).

[30] Senthil, P., E.C.G. Signals Application Automated Apprehension and Allocation of Cardiovascular Abnormalities, Asian Journal of Electrical Sciences (AJES).5(2) (2017) 28-32.

[31] Senthil, P., Evolutionary Algorithms Techniques Based on M.E.T. Heuristics of Accustomed Computing Performance, Asian Journal of Computer Science and Technology.6(1) (2017) 21-26.

[32] Senthil, P., Inheritance Classification Based Artificial Reproduction Analysis and Artificial Neural Networks (Icarus), Asian Journal of Computer Science and Technology. 6(1) (2017) 6-14.

[33] P, Senthil., FOURIER TRANSFORM BASED CLASSIFICATION ABORIGINAL ALGORITHM, Asian Journal of Science and Applied Technology (AJSAT).6(1) (2017) 5-9.

[34] P, Senthil., Graphics in Combination Handguns Preparation Classification (Gaps), Asian Journal of Engineering and Applied Technology (AJEAT). 6(1) (2017) 1-9.

[35] Yang H, Marzetta T., Total energy efficiency of cellular largescale antenna system multiple access mobile networks, In: Proc IEEE Online Conference on Green Communications(2008) Smart 2020: enabling the low carbon economy in the information age, The Climate Group and Global e-Sustainability Initiative (GeSI).

[36] Wiesel A, Eldar Y, Shamai S., Linear precoding via conic optimization for fixed MIMO receivers, IEEE Trans Signal Process. 54(1) (2006) 161–176.

[37] Tugnait JK, Tong L, Ding Z., Single-user channel estimation, and equalization, IEEE Signal Process Mag. 17(3) (2000) 16–28.

[38] Cui S, Goldsmith A, Bahai A., Energy-efficiency of MIMO and cooperative MIMO techniques in sensor networks, IEEE J Sel Areas Commun 22(6) (2004) 1089–1098.

[39] Wolniansky PW, Foschini GJ, Golden GD, Valenzuela RA., V-BLAST: an architecture for realizing very high data rates over the rich-scattering wireless channel, In: Ursi International Symposium on Signals, Italy.(2002) 295–300.

[40] Joung J, Sun S ., Two-step transmit antenna selection algorithms for massive MIMO, In: IEEE International Conference on Communications (I.C.C.), Kuala Lumpur, Malaysia.(2016) 1–6.

[41] Abhinav Johri, Farooq Husain and Ekta Agarwal., A Review: Visible Light Communication using MU-MIMO-OFDM, SSRG International Journal of Electronics and Communication Engineering. 4(4) (2017) 16-20.